ENGINE/AIRFRAME INTERFERENCE ON TRANSPORT AIRCRAFT WITH DUCTED PROPFANS - THE EUROPEAN RESEARCH PROGRAM DUPRIN -

W. Burgsmüller - Deutsche Aerospace Airbus (DA), Bremen, Germany
H. Hoheisel - DLR, Institut für Entwurfsaerodynamik, Braunschweig, Germany
J. W. Kooi - German-Dutch Wind Tunnel (DNW), Emmeloord, The Netherlands

Abstract

The cooperative European research program DUPRIN (DUcted PRopfan INvestigations) was started by mid 1990 under Area 5-Aeronautics of the CEC frame program BRITE/EURAM. Main purpose of DUPRIN is to build-up the know-how basis, necessary for the new engine types, currently under development. These engines are characterized by very- respectively ultra-high bypass ratios (VHBR/UHBR), coupled with increasing nacelle diameters and hence requiring a closer coupling with the wing. Based on an existing wind tunnel complete-model of a typical twin-engine transport aircraft, plus one ducted propfan and one turbofan engine simulator, the experimental part of DUPRIN was concentrating first on the completion of the missing hardware. Due to this, a second engine simulator of each type was designed and manufactured. Following the preparation of the model, first wind tunnel tests were performed in the German-Dutch Wind Tunnel (DNW). In relation to the turbofan, the results with the ducted propfan showed an increase in installation- as well as in jet-interference drag. The installation effects were spreading over the major part of the wing span. The experimental results were in good agreement with those from the CFD-part of the program. Further detailed investigations of engine installation phenomena are planned within DUPRIN II, started in Spring 1994.

Notations, Indices

c	Wing chord
s	Wing span
x	Chord direction
y	Span direction
C_T	Thrust coefficient
ϵ	Mass flow ratio
F_{18}	Fan exit momentum
F_N	Engine net thrust
K_2	Axial force
C	CRISP, CRUF
E	Engine
HL	Highlite
M	Model
N	Net
T	Turbofan

1. Introduction

The general interest of the aircraft industry to produce and sell competitive products, strengthening environmental requirements concerning reduction of noise and emissions as well as cost reduction due to lower fuel consumption are the major driving forces to improve the quality of new and existing airplanes. Concerning the engine industry, these requirements currently lead to the development of new engine families with very- resp. ultra-high bypass ratios (VHBR/UHB), coupled with increasing nacelle diameters. In context with the requirements concerning minimum ground-clearance and avoidance of increasing length and hence weight of undercarriages this leads to the necessity of a close coupling between wing and engine.

The current knowledge about the related aerodynamic phenomena and their control is limited. This poses the risk that the gains in fuel efficiency of new engine types are lost or even overruled by losses due to negative engine/airframe interference effects.

On this background and in view of current developments in the engine industry aiming at ducted propfan engines the program DUPRIN was started on 1.7.90 with eight Partners, four Associated Contractors and five Subcontractors out of seven EC-countries under coordination of Deutsche Aerospace Airbus.

Main objective of DUPRIN is the joint European

effort of industry, research institutes and universities to develop and use the experimental and theoretical tools in order to build up the necessary data base for installation effects of modern ducted propfan engines on transport aircraft in relation to conventional turbofans.

Phase I of DUPRIN, which was completed in Autumn 1993, covered an experimental as well as a numerical part [1,2].

The experimental part was based on an existing complete-model of a modern transport aircraft, owned by DLR and one engine simulator each, representing respectively a turbofan and a ducted propfan engine class. Within the program, a second simulator of each type was built and finally, a first test was performed in the German- Dutch Wind Tunnel DNW, on the model with ducted propfans and, as reference configuration, with turbofans.

The numerical part of the program was aiming at the application and validation of existing computational fluid dynamic codes (CFD) plus the integration of an improved jet model into the existing Euler code. These theoretical tools can later be used for the optimization of the complex wing/nacelle/engine flow field.

2. Experimental Set-up

2.1 The Wind Tunnel

The German-Dutch Wind Tunnel is an atmospheric single return wind tunnel. The main dimensions of the wind tunnel are given in Figure 1. As shown in Figure 1 the wind tunnel has interchangeable test sections. In total there are two test sections, one with a fixed cross section of 9.5 x 9.5 m^2 and one with a convertible cross section. This convertible test section has side walls which can be moved inwards to reduce the cross section from the maximum size 8 x 6 m^2 to the minimum 6 x 6 m^2. This latter configuration was used in the present test. The maximum velocity for the three test sections are 62 m/s, 116 m/s and 152 m/s respectively.

For models equipped with an internal balance a sting support system is used [3]. This sting support enables to vary the angle of attack of the model from -15° to +45°. Yawing angles can range from -30° to +30°. During an angle of attack sweep the sting support moves vertically in order to keep the model reference position as close as possible to the centre of the test section. The whole sting system operates under computer control.

Drive air for engine simulators is obtained from a compressor plant. The plant has two compressor sets, which each deliver 3 kg/s at 280 bar, and a set of steel bottles to store the compressed air. After compression the air is cooled and dried to a dew point of at least 200 K. For compressed air driven engine simulators dry air is of utmost importance, while a too high humidity will lead to ice formation in the exhaust nozzle.

The compressed air is transported to the test section via two separate supply lines. Each line has a computer controlled regulating valve. Either the simulator rpm or the pressure at any point in the supply lines downstream of the valve can be kept constant. As the pressure drop over the valve cools down the air it is necessary to heat up the air again. To this end each line has a heat exchanger.

The mass flow to the simulator turbines is measured by means of sonic venturies in the supply line.

2.2 Model Description

The model configuration considered in this study is a twin-engine aircraft which represents a typical modern wide-body transport aircraft of Airbus type. Compared with the Airbus A320 the model scale is about 1:10. The design Mach number of the wing is $M_\infty = 0.785$ at a lift coefficient of $C_L = 0.5$. The main geometrical data of the model are the following:

- Fuselage diameter d_F = 0.434 m
- Total wing area A_W = 1.266 m^2
- Leading edge sweep φ = 27.1°
- Quarter chord sweep φ_{25} = 25.0°
- Wing dihedral φ_D = 4.8°
- Aspect ratio Λ = 9.35
- Taper ratio λ = 0.3

The shape of the fuselage is defined by a forebody including a cockpit, a cylindrical part containing the wings and an afterbody.

The specific model described above was designed and manufactured by DLR Braunschweig and is called ALVAST. Figure 2 presents a view of the model in tail-off configuration including the main geometrical dimensions and the positions of the engines. Boundary layer transition is fixed by carborundum in the nose region of fuselage, wings and nacelles. The surface pressure is measured on the starboard wing in seven sections D1 to D9 and

on the port nacelle in three sections. Forces and moments were measured by the internal six--component balance 616, which was specially prepared for this model. Pressurized air was supplied by two lines with each three airline bridges for driving the engine simulators. Electronic scanners were installed in the fuselage nose. For the first tests, described below, only the wing in cruise configuration was available, i.e. without any high-lift devices.

Figure 3 shows the ALVAST-model equipped with two conventional turbofan simulators mounted by a dorsal sting in the test section of the DNW. Figure 4 shows the ALVAST-model equipped with the counter-rotating engine simulators representing an ultra-high bypass engine type.

2.3 Engine Simulators

2.3.1 Turbofan engine

For the simulation of this engine type as well as for the ducted propfan the wind tunnel model was equipped with so-called TPS (Turbine Powered Simulator) units. A TPS generally consists of a fan, which is connected to a turbine, driven by pressurized air. In case of the turbofan simulator, fan and turbine are directly connected without any gear (Figure 5). One simulator of this type already existed prior to DUPRIN. The TPS fan casing diameter is 6.4". Further data are given in Table 1.

The first simulator had been designed mainly and manufactured partly in the USA, while assembly and testing had been done by DA in Germany. Following some minor design modifications, the second unit within DUPRIN was completely made by DA and a subcontractor, also including the instrumentation rakes behind fan and turbine, necessary for thrust accounting during the wind tunnel test.

To simulate a turbofan engine, the TPS has to be equipped with fan- and core-cowlings plus a pylon. These components were manufactured by DLR.

After assembling of all model engine components and a final check-out, the complete units were sent to the National Aerospace Laboratory NLR for calibration.

2.3.2 Ducted propfan

For the simulation of an ultra high bypass-ratio engine a new type of simulator named CRUF (for Counter-Rotating Ultra-high Bypass Fan) was developed in cooperation of DLR [4] and the US company Dynamic Engineering Inc. (DEI) and it was manufactured by DEI. This type of simulator is based on the CRISP-concept of MTU München [5]. The simulator consists of the following main parts (Figure 6):

- Counter-rotating fan with eight blades per row, having a tip diameter of 254 mm. Blade design was made by MTU.
- Reversing gearbox
- Air-driven four-stage turbine
- Slim 3D-nacelle

At design speed of 16350 rpm the simulator generates a net thrust of 1150 N at the freestream Mach number of 0.18. Further data of the simulator are given in Table 1.

Parameter	TPS	CRUF1
Simulated bypass ratio	5.	23.
Fan pressure ratio	1.67	1.21
Fan nozzle exit Ma	0.89	0.56
Fan mass flow, kg/s	2.95	7.95
Turbine mass flow, kg/s	1.5	1.5
Fan power requirement, kW	180.	162.
Turbine inlet pressure, bar	20.	20.
Data related to wind tunnel Ma	0.	0.176
Rotational speed, rpm	49,000	16,350

Table 1: Engine simulators for DNW-tests

In the program DUPRIN a second CRUF unit was designed and manufactured by TECHNOFAN (France), based on the DLR specification. Both units contain fan blades manufactured by NLR and each is equipped with a nacelle specially designed for this type of simulator [6]. After final checkout the simulators were calibrated by NLR in order to allow the calculation of the actual thrust during the wind tunnel tests.

3. Wind Tunnel Tests

3.1 Test Program

General intention of the wind tunnel tests was to give a first insight into the installation effects in context with the new class of ducted propfans in

relation to the conventional turbofans. For this purpose three different configurations had to be tested:

- model without engines (WB)
- model with turbofans (WB-TF)
- model with ducted propfans (WB-CRUF)

The tests were done in two campaigns, the first of which covered the tests with turbofans (October 1992), while the second (July 1993) was concentrating on the ducted propfan engines. As a reference, in both campaigns the model without engines was tested.

The test program covered force and pressure distribution measurements for different Mach numbers and incidence angles. Furthermore, the engine power setting was varied.

Generally, the tests are to be seen as a basic investigation, i.e. more detailed tests on the wing with high-lift devices in the low-speed range as well as high-speed investigations are necessary to complete the data base. These investigations are planned to be realized in a later phase of DUPRIN.

3.2 Engine Flow Simulation

For tests with propulsion simulation in the wind tunnel, the model engine must have been calibrated for the delivered thrust and fan main flow over its entire operating envelope. These data are needed to derive the aircraft aerodynamic loads from the wind tunnel balance overall forces. Both types of engine simulators, the turbofans and the CRUF's, were calibrated in the Engine Calibration Facility (ECF) of NLR [7]. For this procedure, the simulators were equipped with special instrumentation [8]. As an example Figure 7 shows for the CRUF simulator the fan nozzle discharge coefficient as a function of the fan nozzle pressure ratio.

$$C_{dF} = \frac{\dot{m}_F}{\dot{m}_{Fid}} \qquad (1)$$

which is defined as the measured fan mass flow divided by the ideal fan mass flow. In addition the engine velocity coefficient

$$C_{vEng} = \frac{K2}{\dot{m}_F\, v_{jFid} + \dot{m}_C\, v_{jCid}} \qquad (2)$$

which is defined as the measured gross thrust (balance), divided by the ideal thrust (actual mass flow multiplied with fully expanded ideal velocities). The data are from two runs for one Mach number in which RPM was step-wise increased and decreased. The repeatability of these coefficients are clearly of the order of 0.25% and acceptable.

The turbine powered simulator (TPS) technique used for experimental investigations on airframe/-engine interference problems has some deficiencies. The main deficiency of the TPS is the too low core temperature due to the expansion of the compressed air, and hence the core jet velocity. Investigations of the jet temperature effects for an isolated bypass engine simulator have shown that for normal engine operating conditions the difference between cold and hot core flow simulation as regards jet spread and entrained mass flow is small [9]. Therefore, it is common practice to operate the TPS with the correct fan exit Mach number compared to those of the real engine. In the present case with the new type of engine with ultra high bypass ratio another similarity rule was applied. Because of the cruise - configuration of the wind tunnel model the net thrust of the two types of engine has to be

$$F_{NTE} = F_{NCE} \qquad (3)$$

Concerning the fan exit momentum the following ratio should be fulfilled

$$\frac{F_{18CE}}{F_{18TE}} = \frac{F_{18CM}}{F_{18TM}} \qquad (4)$$

Combining both requirements leads to the fan exit momentum of the two different models, namely

$$F_{18CM} = \frac{K_C}{K_T}\, F_{18TM} \qquad (5)$$

with the thrust ratio for the turbofan

$$K_T = \frac{F_{18TE}}{F_{NTE}} \qquad (6)$$

and the thrust ratio for the CRISP

$$K_C = \frac{F_{18CE}}{F_{NCE}} \quad (7)$$

as the ratios of the real engines. That means, the CRUF's have to be operated in such a way that the ratio of the fan gross thrust F_{18CM} and total engine net thrust F_N is equal to the one of the real engine at design condition. The realized ratio F_{18} to F_N is demonstrated in Figure 8 in comparison to the given data of the real engines for the investigated Mach number range. The comparison of simulated data with the engine data looks very good. Also the net total thrust of the two CRUF simulators is in good agreement as demonstrated in Figure 9. The realized parameters in the present investigation are given in Table 2.

Simulator	TF	CRUF
$C_{TN, MTO}$	0.21	0.19
$\epsilon_{HL, MTO}$	1.18	1.12
$\epsilon_{HL, TFN}$	0.36	0.60

Table 2: Realized parameters

4. Experimental Results

4.1 Global Engine Interference Effects

In this section the overall effects of the propulsion units on the total forces are described, in particular lift and drag as deduced from the balance measurements. As a typical result concerning the overall engine installation effects Figure 10 shows lift and drag for the two different types of engines (WT-TF and WB-CRUF) in comparison with the model without engines (WB), at maximum take off power (MTO). The development of lift versus incidence is almost linear but the installation of the engines generally leads to a decrease of lift. For the conventional turbofan, the loss of lift due to the engines is nearly constant for the most interesting range of α between $0° < \alpha < 8°$. In the case of the CRUF-engine, however, the loss is disappearing with increasing incidence, probably due to the lift increase of the nacelle, which is greater for the CRUF than for the turbofan.

The polars C_L (C_D) show an important increase of the drag due to the presence of the engine. In particular the new UHB-engine type CRUF leads to an additional increase of drag compared to the turbofan in the most interesting range of lift $0.4 < C_L < 0.7$. A more detailed analysis of this interference effects shows the influence of the power setting on drag, i.e. the jet-interference drag as defined by

$$C_{DJ} = C_{DMTO} - C_{DTFN} \quad (8)$$

Figure 11 shows for a constant Mach number and incidence the effect of C_{DJ} for the two different types of engines. Starting from the corresponding drag level at through-flow nacelle condition (TFN) where the nacelle exit velocity is equal to free stream velocity, the drag increases due to the jet effects up to the level at maximum take-off power (MTO). As mentioned above, MTO power levels represent the necessary ratio of F_{18}/F_N (see Figure 8) for the two different types of engines. In the case of the turbofan, the jet interference drag increases in a step beyond TFN conditions, is then nearly constant up to about 75% of MTO-power and from thereon further increases up to MTO-power. In the case of the CRUF, the increase at lower power-setting is in agreement with the turbofan. However, the drag creep starts already earlier at about 45% of MTO-power with a gradient comparable to the turbofan. Due to this, the jet influence on the drag between the two engine types in that condition is nearly constant and in the order of 8 to 10 drag counts.

4.2 Local Lift Behaviour on the Wing

The local lift distribution in spanwise direction is shown in Figure 12 for the different engine configurations for MTO-condition in comparison to the wing-body configuration. The engine installation affects the lift distribution over the whole span, with greater losses in the case of the CRUF-engine. The engine jet effects are limited to about 60% of span. The remarkable lift loss in the case of CRUF is generated in particular in the inboard region due to the jet-effect (Figure 13). The jet-influence in the case of the turbofan is smaller and existing on inboard and outboard side of the pylon.

To get more detailed information on the interference effects, the flow field will be analyzed using the wing pressure distribution. At TFN condition (Figure 14), the installation effects on the upper surface of the wing are identical for both engines, while on the lower surface the CRUF installation leads to slightly higher lift-losses in the front part of

the chord length, compared with the turbofan. For MTO condition (Figure 15) the effects on the upper surface are unchanged, while especially in case of CRUF a lift-loss is occurring at the inboard side of the pylon. The jet-effect of the two types of engines is separately shown in Figure 16, with a remarkable influence on the inboard side of the CRUF only.

5. Computational Investigations

Besides experimental investigations the analysis of interference effects is performed by numerically solving the Euler equations.

5.1 Solution Method and Grid Generation

The solution scheme applied is the DLR code CEVCATS. The code requires body-fitted structured meshes. The discretization is performed using a central differencing cell vertex finite volume scheme with artificial dissipation. For time integration an explicit Runge-Kutta scheme is employed, and convergence towards steady state is accelerated using local time stepping, implicit residual averaging and multigrid. The code is written in a block-structured form and allows an arbitrary application of boundary condition on the block faces [10]. Since the CEVCATS code is basically designed to solve for compressible flows, it was checked on experimental results of transonic flow conditions for a comparable complex configuration under investigation [11].

The necessary grid generation was performed using body-fitted, block-structured meshes. Using the grid generation concept of [12] an H-type grid structure in streamwise direction and an O-type structure in spanwise direction was employed for the wing-body combination. Engine and pylon are integrated into this basic grid by introducing a sub-block containing these components. A three-dimensional view of the field grid around the ALVAST-configuration with engines is shown in Figure 17. Figure 18 gives a view of a cross section of the field grid at the pylon location for the two different types of engines under investigation. The complete field grid consists of eleven computational blocks with about 600,000 cells.

Using the solution of the Euler equations offers certain advantages and short comings, which shall be discussed prior to the presentation of results to avoid any misinterpretation. One advantage of the solution of the Euler equations with respect to the potential flow model is that the former is exact for inviscid flows, i.e. mass, momentum and energy are conserved. Secondly, in case of solving the Euler equation, the vortex sheet behind a lifting wing needs not to be specified. Furthermore, the shape of an inviscid jet comes out of the solution and no assumptions are at prior necessary. However, neglecting the viscous effects causes more or less distinct and systematic deviation between experimental and computational results. In particular for the assessment of interference phenomena the jet effect has to be considered. For this reason, the activity of TU-Berlin is concentrated on the coupling of the DLR grid generation procedure and the DLR-Euler-code with a finite difference viscous jet method. For the investigated configuration this method is in advanced development phase. In the present investigation an actuator disk has been used to establish the jet boundary conditions. The pressure ratio at the out-flow face was specified. The incoming mass flow was prescribed with a stream tube area ratio ϵ_{HL}.

5.2 Results

Corresponding to the wind tunnel tests different Euler calculations have been performed. As an example Figure 19 shows at the free-stream Mach-number M = 0.27 and $\alpha = 4°$ the wing pressure distribution for the important sections in the vicinity of the engine for the two different engines plus the case without engine. In all cases the engine installation leads to a significant reduction in the wing leading edge suction peak and increasing pressure on the wing upper surface. The UHB-configuration causes lower pressure on the lower wing surface compared to the turbofan, thus the additional lift reduction occurs at the engine position. Note, that this behaviour was already observed in the experimental results.

Figure 20 shows direct comparison of experiments and computational data of the wing pressure distrubution of the ALVAST model with the CRUF engine configuration for M = 0.27 and an angle of attack $\alpha = 4°$. For the TFN-condition of the engine (upper diagrams) the comparison reveals for the inboard position a good agreement between the measured and calculated results. At outboard position small differences on the lower side of the wing can be observed. In the case of MTO-condition (diagrammes below) the comparison between experiments and calculated results looks also good, however the local lift is overpredicted by the theory due to the neglection of viscosity, as shown in Figure 21. Qualitativly, the calculation of the wing pressure distribution agrees well with the experiments. That means, the solution of the Euler

equation model interference phenomena in this particular low-speed case.

6. Conclusions

The intention of the work under DUPRIN I, described above, was to provide an experimental and theoretical basis for later, more detailed experimental and theoretical investigations, in order to build up a complete data base concerning installation effects of modern engines on transport aircraft.

Within this context, all items planned under DUPRIN have been completed successfully and the participants formed a very cooperative and effective team.

The results of the basic wind tunnel tests show remarkable differences in the installation phenomena of a CRUF in relation to a turbofan, which are in good agreement with the CFD-results.

In the meantime, the core of the existing team, together with some new participants, has started DUPRIN II, covering the major part of low-speed tests on high-lift configurations accompanied by continuing theoretical work plus the design of simulators also for the new class of very-high bypass-ratio engines (VHBR). These shall be manufactured and used together with the existing hardware for detailed high-speed investigations in a later phase III of DUPRIN.

7. Acknowledgement

The DUPRIN project was generously supported by the European Union. Dr. R. Dunker of the Directorate General for Science, Research and Development was the EU Project Monitor. His advice and guidance is well appreciated.

The DUPRIN team's dedication and willingness to cooperate contributed in large to the success of the project. The authors acknowledge the advices and helpful support from colleagues at DLR, DNW and NLR.

The authors are grateful for the permission of the EU, the Partners and Associated Partners for the permission to publish this paper.

8. References

[1] Burgsmüller, W.
Preparation and Use of an Existing Wind Tunnel Model for Ducted Propfan Investigation (DUPRIN).
Proceedings Aeronautics' Days, Brussels (1991).

[2] Burgsmüller, W.; Hoheisel, H.; Kooi, J.W
Results of Engine/Airframe Interference Investigations on Transport Aircraft with Ducted Propfan versus Turbofan Engines.
Conference Proceedings, CEC, Aerodays, Naples (04/05 October 1993).

[3] Burgsmüller, W.; Castan, C.; Kooi, J.W.; Bècle, J.P.
Recent Development in Low-Speed TPS-Testing for Engine Integration Drag and Installed Thrust Reverser Simulation
AGARD Symposium on Aerodynamic Engine/Airframe Integration, Fort Worth, Texas, USA (1991).

[4] Hoheisel, H.
The Design of a Counter Rotating Ultra-High Bypass Fan Simulator for Windtunnel Investigations.
DLR-FB 93-20 (1993).

[5] Grieb, H.; Eckardt, D.
Propfan and Turbofan, Antagonism or Synthesis.
ICAS Paper No. 86-3-8.2 (1986).

[6] Kiock, R.; Hoheisel, H.
Design of the axi-asymmetric Nacelle for the Counter Rotating Ultra-High Bypass Fan Simulator.
DLR-FB 93-52 (1993).

[7] Hegen, G. H.
The NLR Model Calibration Facility Description and Guide for Users.
Preliminary internal document AX-92-082 (1993).

[8] Kooi, J.W.; Kiock, R.; Slauerhoff, J.
Tools for the Experimental Study of the Integration of Ultra-High Bypass Engines on Transport Aircraft.
AIAA94-2562 (1994).

[9] Korus, A.
Experimentelle und theoretische Untersuchungen über den Strahleinfluß bei der Um-

strömung eines Bypass-Triebwerkes.
DLR-FB 93-17 (1993).

[10] Rossow, C.-C.; Ronzheimer, A.
Investigation of Interference Phenomena of Modern Wing Mounted High-Bypass-Ratio Engines by the Solution of the Euler- Equations.
AGARD-CP-498 (1991).

[11] Rossow, C.-C.; Godard, J.L.; Hoheisel, H.; Schmitt, V.
Investigations of Propulsion Integration Interference Effects on a Transport Aircraft Configuration.
AIAA 92-3097 (1992).

[12] Rossow, C.-C.; Ronzheimer, A.
Multi-block Grid Generation Around Wing--Body-Pylon Configuration.
Conference proceedings on Numerical Grid Generation in Computational Fluid Dynamics, Barcelona, Spain (03-07 June, 1991).

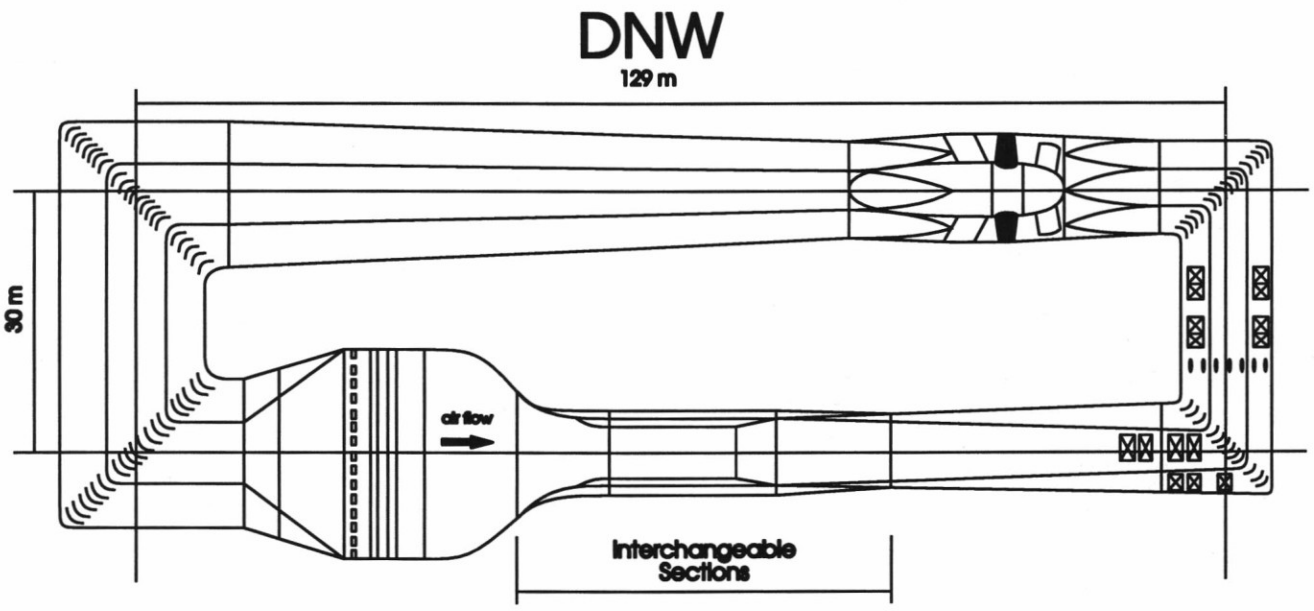

Figure 1: The airline of the DNW

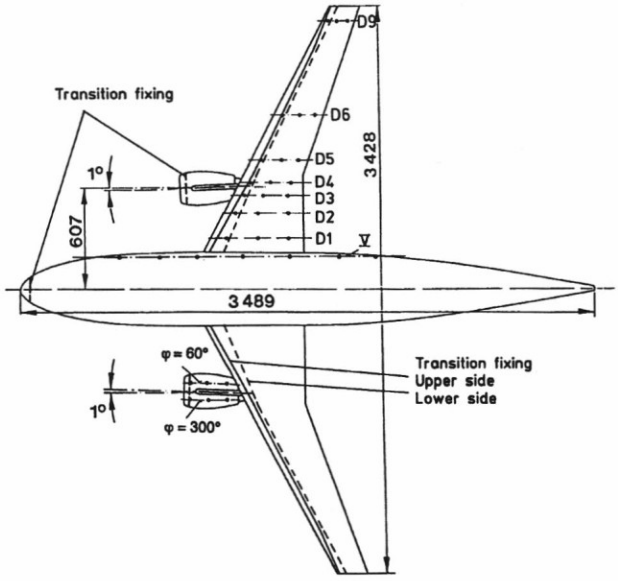

Figure 2: Top view of the ALVAST model

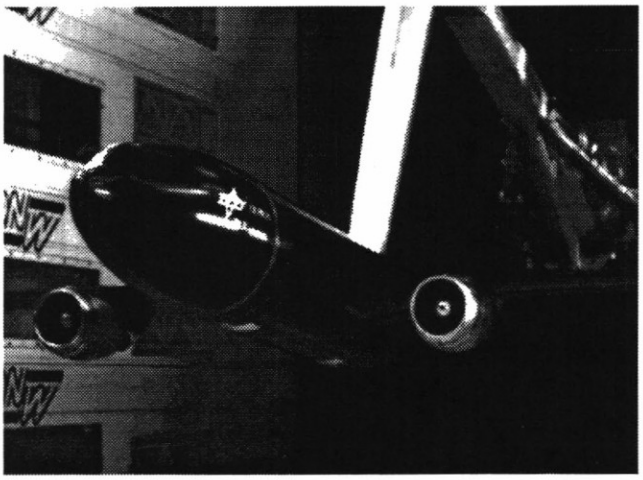

Figure 3: ALVAST-model with turbofan simulators in DNW test section

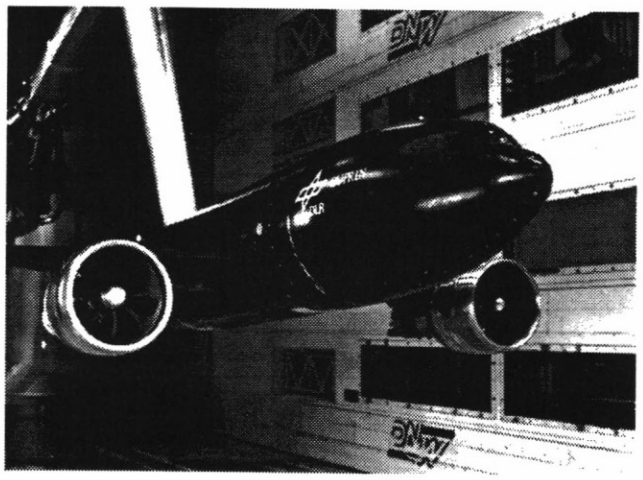

Figure 4: ALVAST-model with CRUF simulators in DNW test section

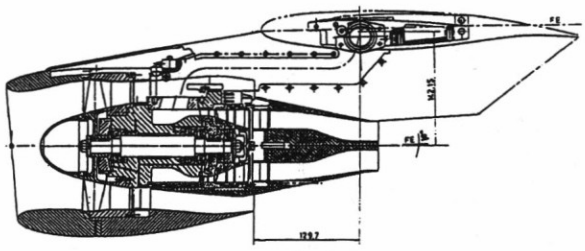

Figure 5: Turbofan simulator

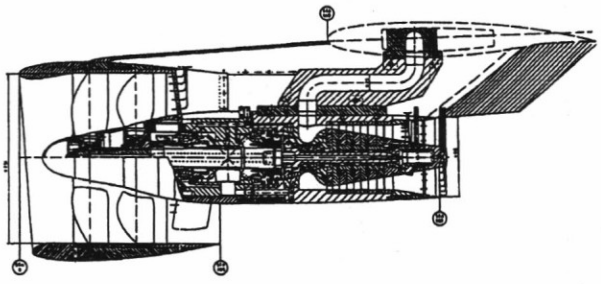

Figure 6: CRUF simulator

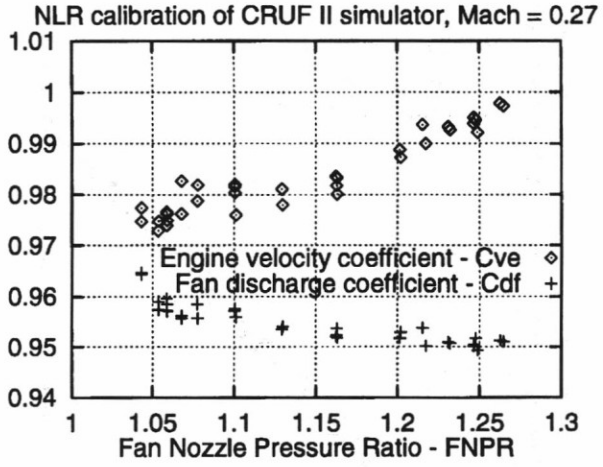

Figure 7: Discharge coefficient C_{dF} and engine velocity coefficient C_{vE} versus fan nozzle pressure ratio for CRUF, M = 0.27

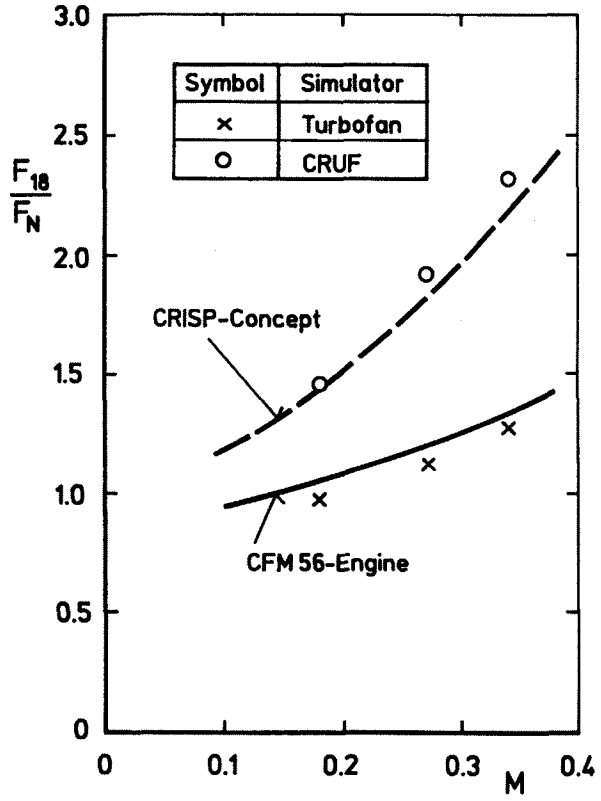

Figure 8: Ratio of fan exit momentum to total engine net thrust versus free-stream Mach number

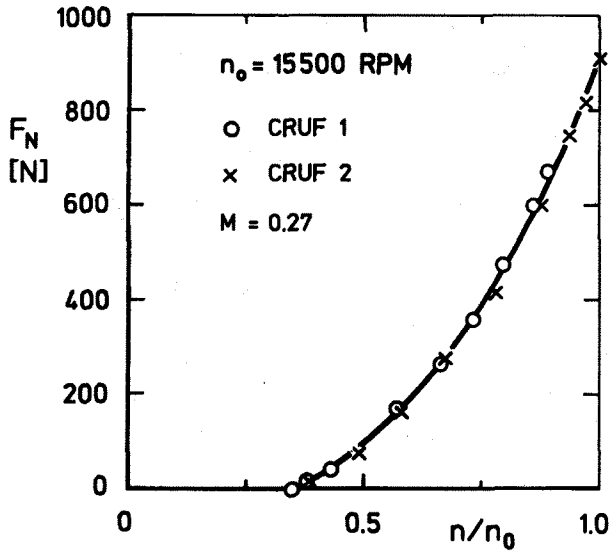

Figure 9: Net thrust CRUF1 and CRUF2 versus reduced rpm

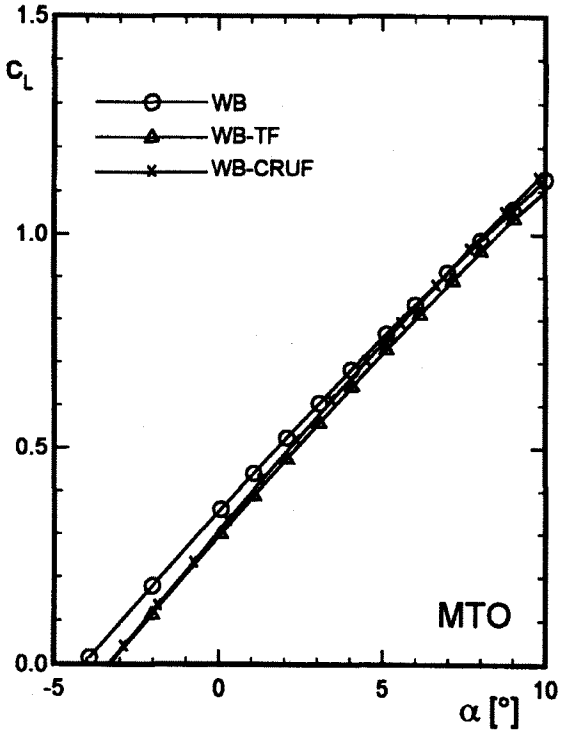

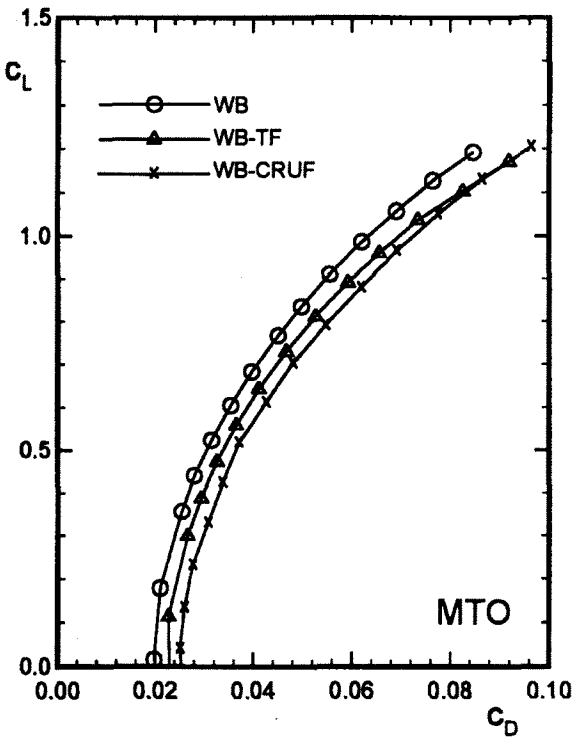

Figure 10: Total force measurements for clean (WB), turbofan (WB-TF) and CRUF (WB-CRUF) configuration, M = 0.27

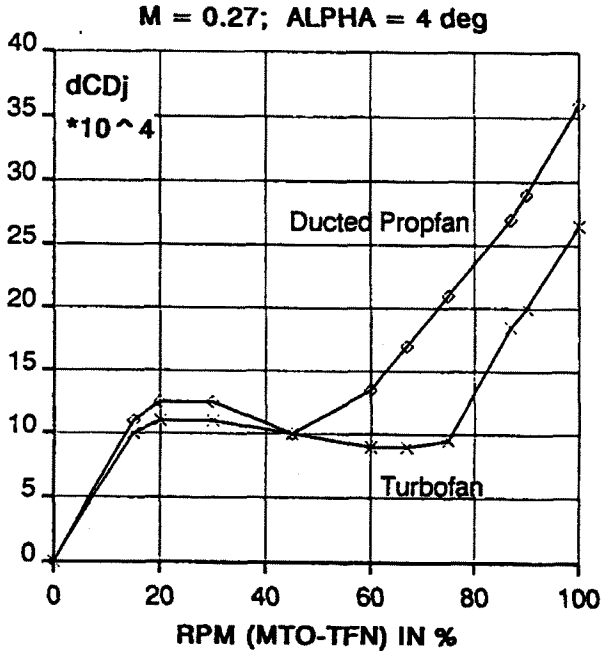

Figure 11: Jet interference effects on drag, M = 0.27

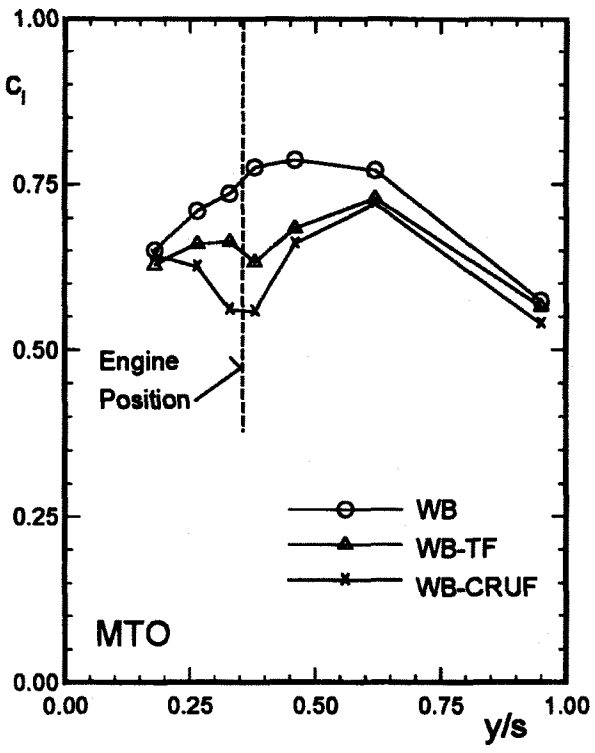

Figure 12: Local lift distributions for different configurations at MTO-condition, M = 0.27

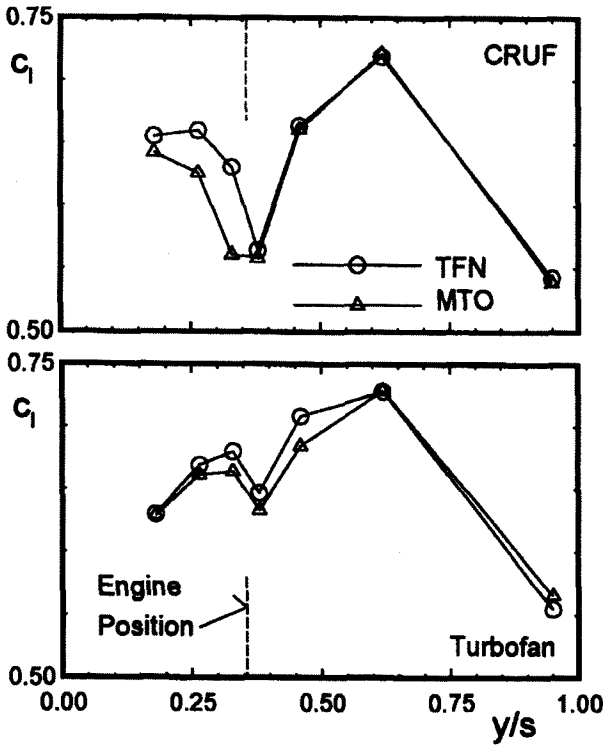

Figure 13: Local lift distribution, influence of power setting, M = 0.27

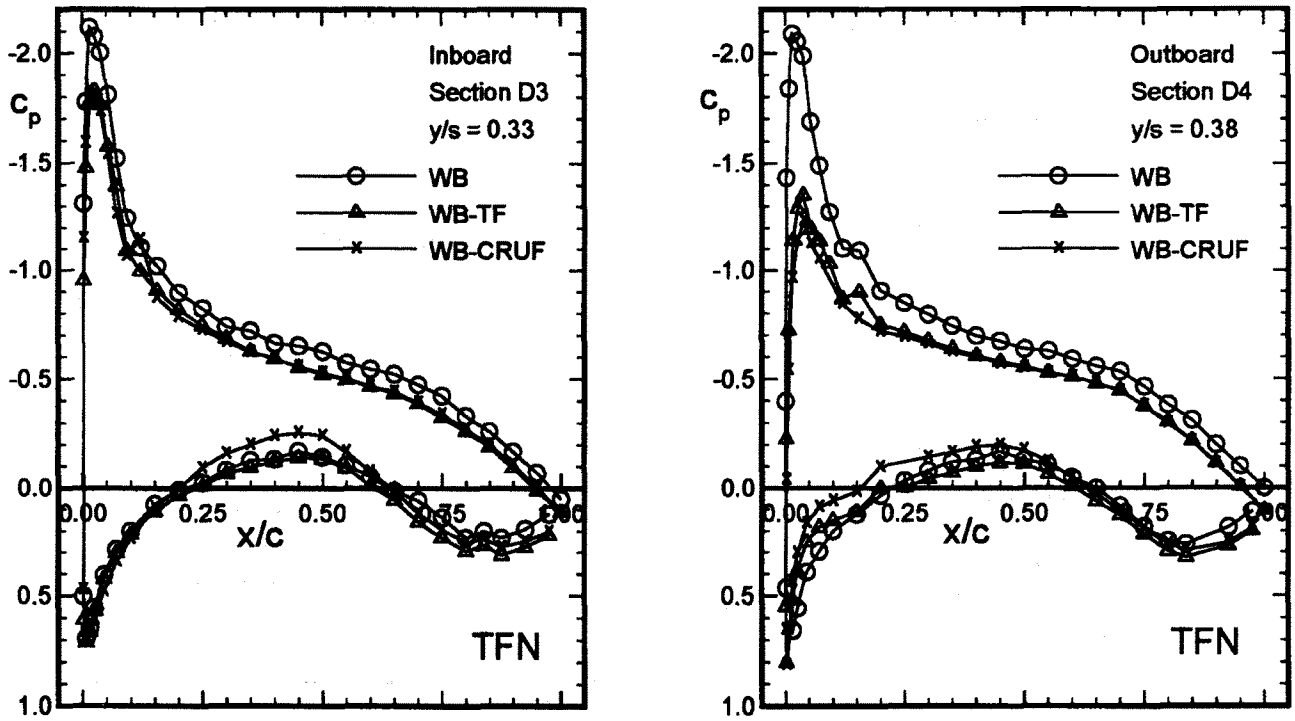

Figure 14: Wing pressure distributions at MTO-condition, M = 0.27, $\alpha = 4^o$

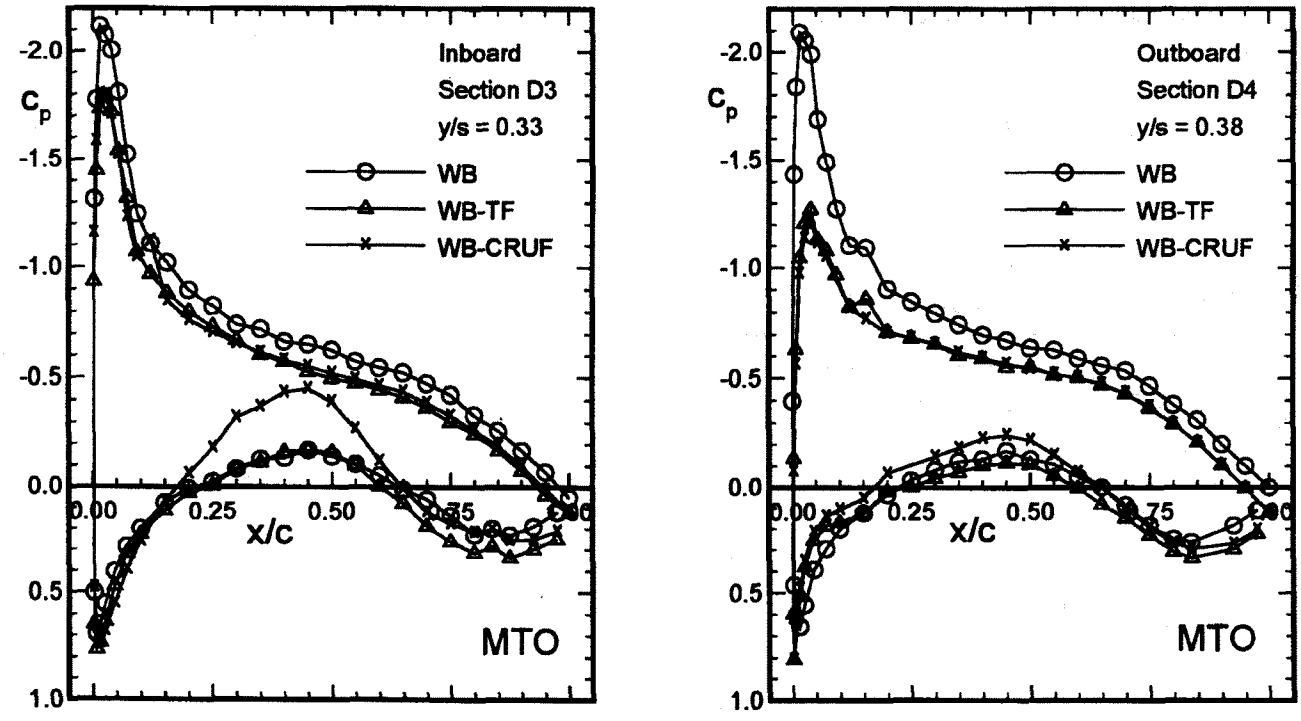

Figure 15: Wing pressure distributions at MTO-condition, M = 0.27, $\alpha = 4^o$

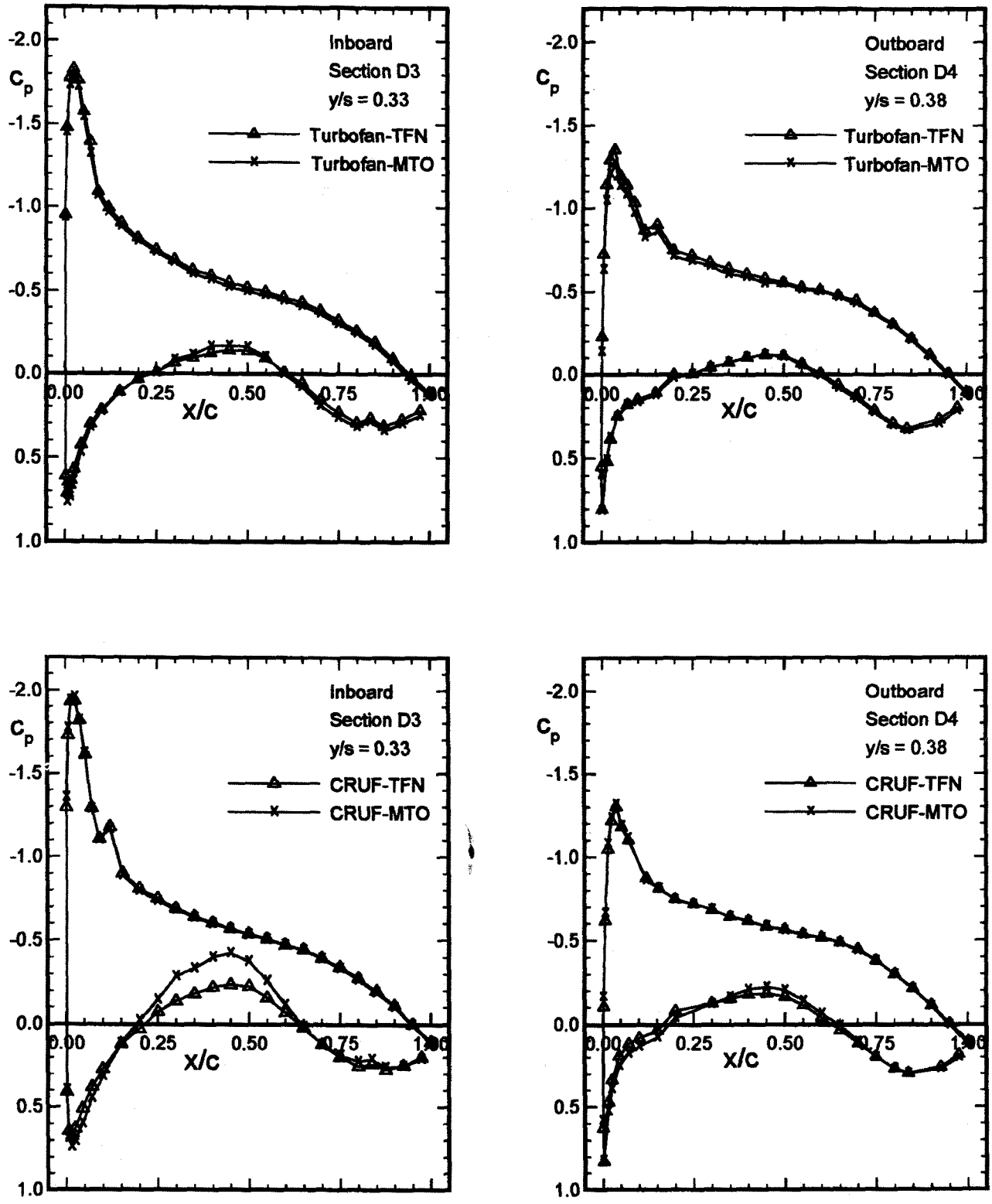

Figure 16: Wing pressure distributions, jet influence, M = 0.27

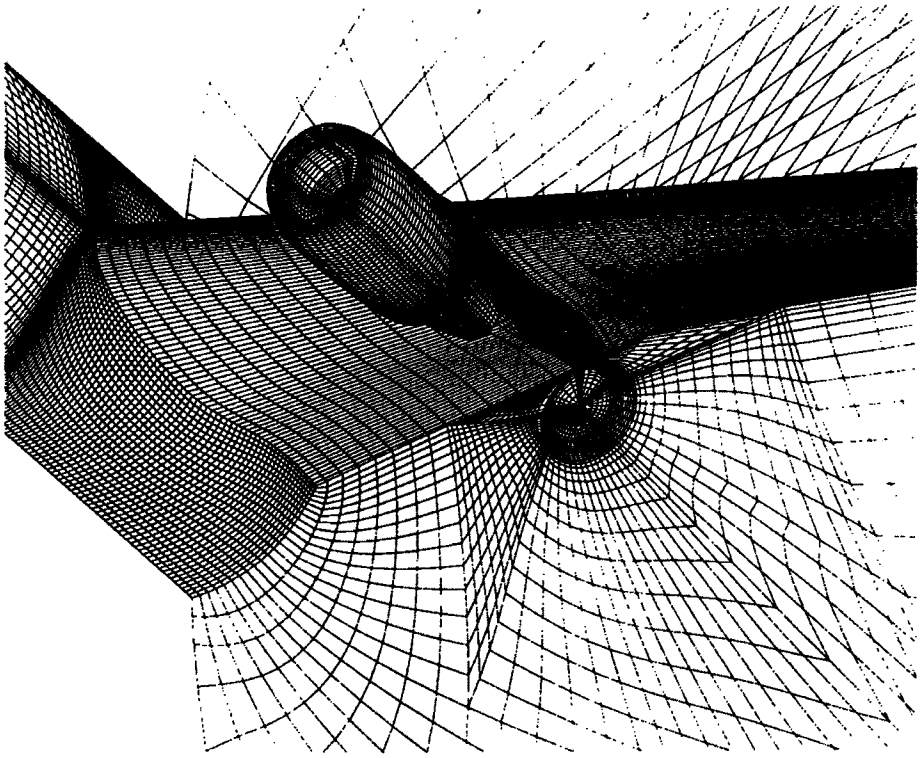

Figure 17: Field grid for configuration with turbofan engines

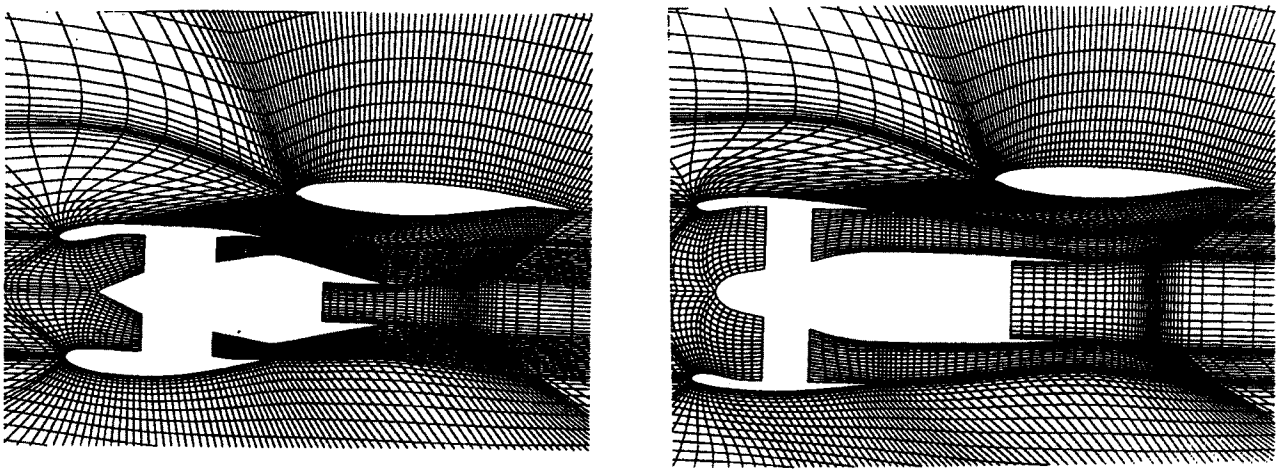

Figure 18: Cross-section of field grid for turbofan and CRUF configuration

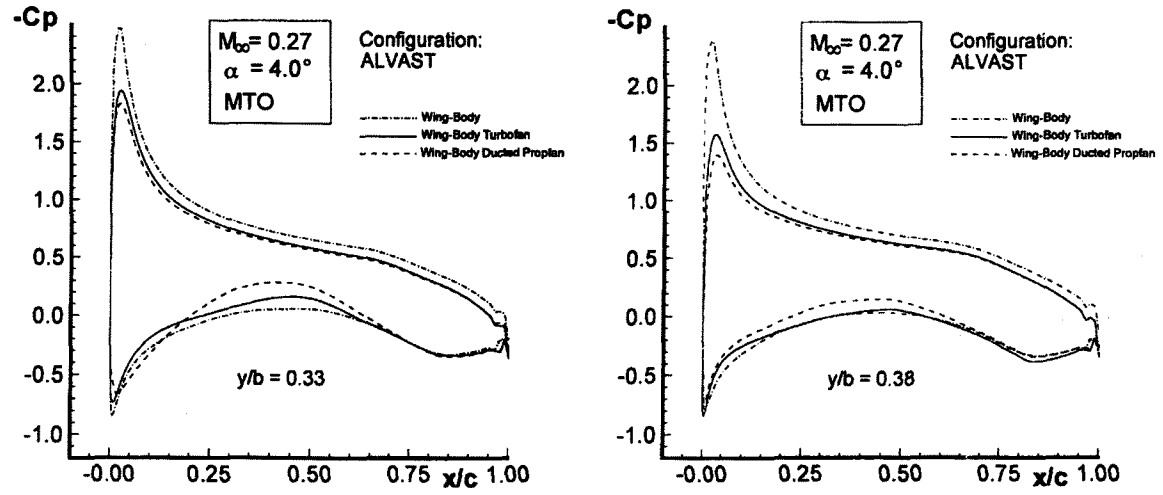

Figure 19: Calculated wing pressure distributions for different configurations

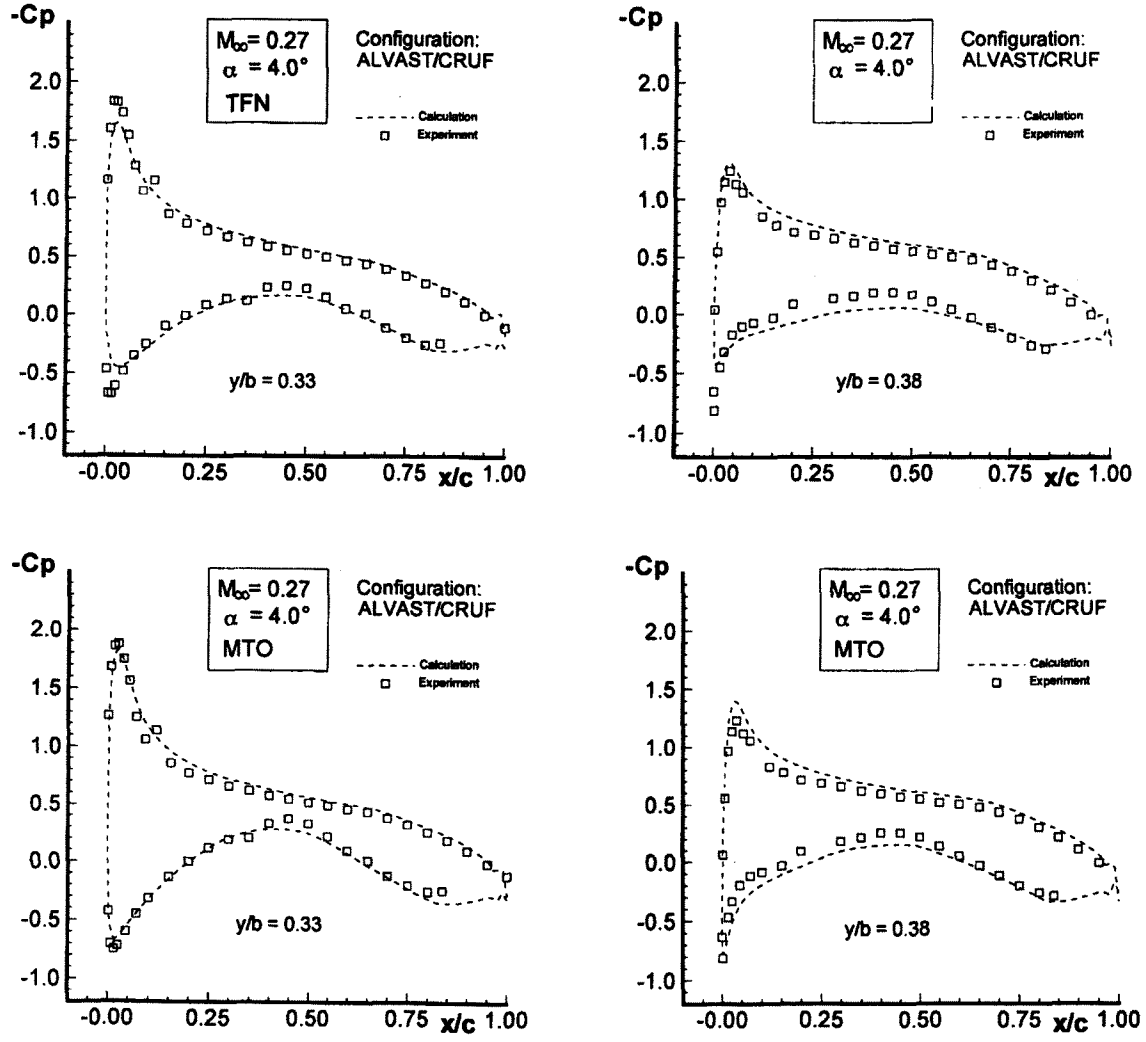

Figure 20: Comparisons of experimental and computational wing pressure distributions for CRUF configurations

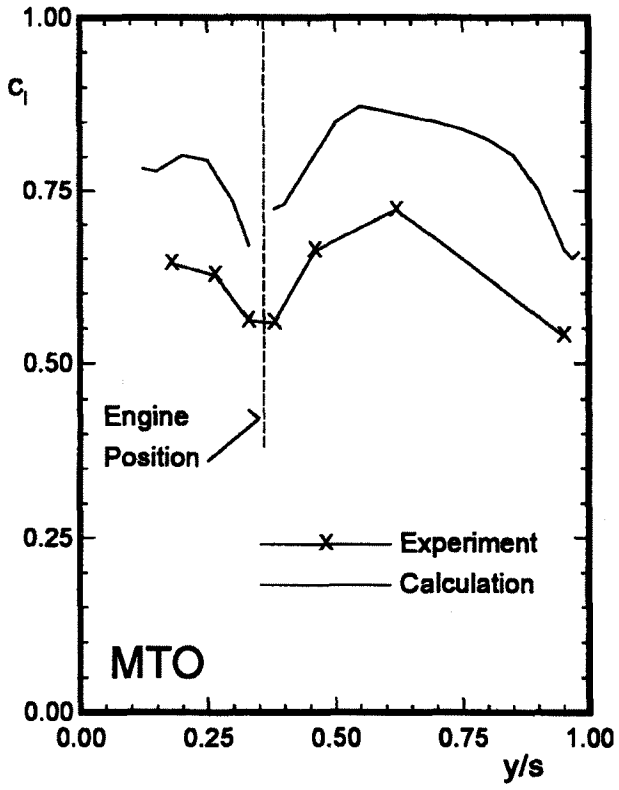

Figure 21: Comparison of experimental and computational local lift distribution for CRUF configuration